EFFICIENT 3D SEISMIC ACQUISITION DESIGN USING COMPRESSIVE SENSING PRINCIPLES

MENGLI ZHANG

Department of Geophysics, Colorado School of Mines, Golden, CO 80401, U.S.A.
menglizhang@mines.edu

(Received May 27, 2023; accepted August 15, 2023)

ABSTRACT

Zhang, M., 2023. Efficient 3D seismic acquisition design using compressive sensing principles. *Journal of Seismic Exploration*, 32: 427-454.

The ability to acquire 3D seismic data efficiently and cost-effectively is a major consideration in many applications. One way to achieve this goal is through the theory of compressive sensing. Compressive sensing uses sparse acquisition designs combined with the post-acquisition reconstruction to reduce the number of sensors. Sensor deployment or sampling pattern is a critical component in compressive sensing. Therefore, we analyze sampling patterns based on a Spectral Resolution Function (SRF) to improve the quality of acquired data. We have investigated two types of sparse seismic acquisition designs that use fewer receivers deployed irregularly, and also have compared three proposed reconstruction methods for each acquisition design. We predict the reconstruction accuracies of these six strategies, and then we verify our prediction using SEAM seismic dataset. SEAM seismic data examples demonstrate three major results: First, irregular line and irregular point patterns have different properties of SRF, and these properties can be applied to improve the accuracy of compressive sensing results. Second, a good combination of acquisition design and post-acquisition reconstruction selected based on the properties of SRF is able to obtain better reconstructed shot gathers and imaging results. Third, numerical simulations show that we can reconstruct single shot gather using only 25% of receivers and then produce seismic migration images comparable to those obtained from the full shot gathers. The overall results indicate that, the combination of a sparse acquisition design and corresponding compressive sensing reconstruction method could help facilitate a new generation of cost-effective seismic acquisitions.

KEY WORDS: acquisition design, compressive sensing, seismic acquisition, reconstruction, 3D.

0963-0561/23/$5.00

INTRODUCTION

3D seismic method is among the most powerful geophysical methods since it can capture accurate geological information and facilitate energy exploration and production. However, 3D seismic acquisitions are costly and time consuming since both expensive sensors and a huge number of receivers are needed. One way to reduce the cost of 3D seismic acquisitions is to develop inexpensive sensors, which is an on-going effort. Meanwhile, an alternative way is to reduce the number of sensors deployed in a survey. The massive number of sensors required comes from the use of dense grids of uniformly placed sources and receivers. Use of uniform and dense sampling designs is dictated by the practical ease of data acquisition and Shannon-Nyquist sampling theory. Shannon-Nyquist sampling theory is based on Fourier data processing and sampling criteria to avoid aliasing, and establishes a sufficient condition for the sample rate to capture the desired information. Therefore, the uniform locations of shots and receivers we apply in 3D seismic acquisition also provide a sufficient condition for obtaining subsurface images. This equal-interval and high-density acquisition strategy ensures high-quality seismic data but incurs a great cost. Equal-interval seismic surveys collect a massive number of samples. This number of samples required by Shannon-Nyquist sampling theory is sufficient, and some of these samples are redundant. It is therefore logical to think that a subset of full Nyquist samples is still able to retain the information we need. Thus, some research has been conducted on how to avoid such an expensive, dense seismic data acquisition mode, and focus on different deployment patterns using fewer receivers and sources.

Compressive sensing (Donoho, 2006; Wakin et al., 2006; Candès and Wakin, 2008) provides such a solution for special deployment patterns. Compressive sensing theory states that it is possible to reconstruct a signal from a sparse set of irregular samples if the signal has sparse coefficients in a transform domain. Compressive sensing has seen successful applications in other fields such as Magnetic Resonance Imaging (MRI) (Lustig et al., 2007, 2008) and single-pixel camera (Baraniuk and Kelly, 2007). These applications show that compressive sensing can reconstruct a signal from a sparse set of samples with irregular intervals (Candès et al., 2006; Wakin et al., 2012) instead of full samples using regular intervals. These developments are highly counter-intuitive to the familiar thinking based on Shannon-Nyquist theory.

Compressive sensing has had successful examples in the medical community (Donoho and Tsaig, 2008; Donoho and Tanner, 2010; Donoho et al., 2012; Tsaig and Donoho, 2006). In exploration seismology, which is costly to acquire data, compressive sensing has also inspired new approaches to data acquisitions (Herrmann, 2009; Janiszewski et al., 2017; Brown et al., 2017; Milton et al., 2012). Simultaneous source acquisition (Mosher et al., 2017, 2012; Li et al., 2017) is one of such applications by

performing source deblending using compressive sensing. This type of acquisition reduces the acquisition time by focusing on the source.

However, in onshore and ocean bottom seismic surveys, the more expensive part is the deployment of dense receivers or nodes. These acquisitions are also faced with the difficulties caused by limited access to deploy sensors on private properties or in difficult terrains or bathymetry. Therefore, trying to develop a more efficient method by working with receivers is a logical route and complements the source-related efficient acquisition methods such as simultaneous sources (Wason and Herrmann, 2013; Abma et al., 2015). We pose the following question: Can we explore different receiver patterns to design sparse acquisitions using fewer receivers and then reconstruct the dense data for next step to use with established processing and imaging methods?

To answer this question, we have developed two types of sparse acquisition designs. For each acquisition geometry, we have also proposed three different reconstruction methods using compressive sensing theory. We then evaluate these six seismic data acquisition methods. Our contributions from this work include defining the sampling pattern analysis and applying these analyses to inform acquisition design and data reconstruction. Moreover, our demonstrations show that it is possible to achieve high-resolution data reconstruction with a low-cost acquisition. Lastly, our research can assist in low-cost acquisitions in seismology including both ocean bottom cable (OBC) and ocean bottom node (OBN).

Our work is divided into two steps, the first step is acquisition design, and the second step is reconstruction. In contrast to the research focusing on compressive sensing reconstruction (Zwartjes and Gisolf, 2007; Zhang, 2020, 2021) using random sampling (Moldoveanu, 2010; Moldoveanu et al., 2018; Zhang and Li, 2021; Zhang, 2022; Zhang and Li, 2022), our work focuses on acquisition design using an information criterion to distinguish between different patterns. Compared with Naghizadeh and Sacchi (2010)' research, our research uses a different combination of the three components in compressive sensing. Our work demonstrates that a good combination can help significantly reduce the number of samples required.

In this paper, we will first introduce two types of sparse acquisition designs and propose three compressive sensing reconstruction strategies for each acquisition design. We then analyze the sampling pattern and predict the reconstruction accuracy among these strategies. At last, we demonstrate our acquisition design and reconstruction strategies on the SEAM seismic data set, and test our prediction on seismic shot gather and imaging results.

TWO SPARSE ACQUISITION DESIGNS

We will investigate two types of sparse acquisition designs. One is to simulate ocean bottom cable (OBC), and the other is to simulate ocean bottom node (OBN). Both have practical applications.

In seismology, we usually deploy the receivers with regular intervals on the earth's surface or ocean bottom, such as illustrated in Fig. 1(a). We obtain a 3D volume from such a full acquisition design, which means the X-, Y-, and t-directions are all fully sampled. we use the term desired full data to represent this hypothetical 3D volume in Fig. 1(a) in this paper. Compared with the easily obtained full samples in the t-direction, full sampling in X- and Y-directions requires a huge number of receivers, and leads to high acquisition costs. To overcome this difficulty, we apply compressive sensing theory to reduce the number of receivers needed.

If we use the receivers affixed on a cable (henceforth reference to as cabled receivers) on such as streamers or OBC, we can deploy these receivers as irregularly spaced lines to form a sparse acquisition as illustrated in Fig. 1(b), where the variable is the line spacing. In this case, we have the full sampling in t- and X-directions marked by lines, and sparse irregular sampling in Y-direction. A compressive sensing reconstruction algorithm can then be used to recover the missing samples.

Besides the cabled receivers, the individually deployed receivers such as single sensors on land and OBN, makes the scattered deployment in 2D possible. Therefore, we can also design a sparse acquisition geometry such as the irregular points illustrated in Fig. 1(c). In this scenario, we have the full sampling in the t-direction marked by the lines, and sparse irregular sampling in X- and Y-directions. Post-acquisition reconstruction algorithm will recover the missing samples.

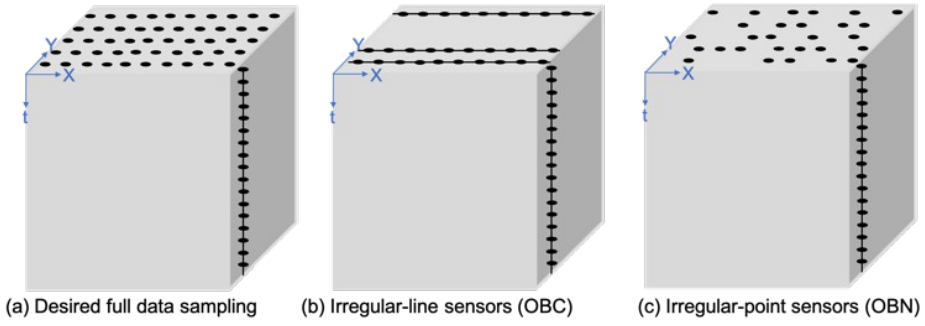

Fig. 1. Conceptual illustration of sparse acquisition designs for 3D seismic data. (a) Desired full data set, and full sampling in three directions; (b) irregular line acquisition, full sampling in t- and X-directions, (b) irregular point acquisition, full sampling in t-direction.

We illustrate these two practical sparse acquisitions respectively by the concepts of irregular line and irregular point survey designs in Fig, 1. For

simplicity, we only plot a line without sample dots if that direction is fully sampled. Since we denote the full samples in a given direction as lines, the full sampled survey lines and the samples in the t-direction are both represented by lines. These 'line' samples are treated the same way in the stage of compressive sensing reconstruction algorithm. Moreover, we will call the two geometry designs irregular line acquisition and irregular point acquisition respectively.

THREE METHODS FOR POST-ACQUISITION RECONSTRUCTION

To obtain the desired fully sampled data in Fig. 1(a), we must first reconstruct such a fully sampled 3D volume from the sparse data acquired from acquisitions in Figs. 1(b) and 1(c), and can then use the reconstructed data in the traditional processing and interpretation. A natural question is how to reconstruct these sparse data volumes? An intuitive approach is to input all the available samples in the sparse 3D volume into the compressive sensing algorithm and obtain the dense data set assembling the desired full 3D data volume. However, besides this strategy of inputting all samples, we propose two more strategies to do the reconstruction. One is to divide the 3D sparse data set into subset of horizontal slices to reconstruct the samples in each subset individually. The other is to divide the 3D data set into subset of vertical slices and do reconstruction of each subset. We will illustration these three reconstruction strategies in the following.

For the irregular line acquisition in Fig. 1(b), we have a limited number of cabled receivers, we deploy these available groups of receivers along irregular lines. Compared with the desired 3D volume with regular full samples in X-, Y- and t-directions, the sparse 3D volume from irregular line acquisition has full samples in one direction and irregular sparse samples in the other direction, such as the irregular lines in these *Y-t* plane and *X-Y* plane. We examine three reconstruction methods illustrated in Fig. 2. Fig. 2(a) illustrates that we reconstruct this data volume with a whole 3D dataset. Fig. 2(b) shows that we subdivide the sparse samples into vertical subsets and reconstruct each subset independently, then we assemble the reconstructed results together to form the reconstructed 3D data. Fig. 2(c) shows that we work in a similar way but group the sparse samples into horizontal subsets.

For the irregular point acquisition in Fig. 1(c), we have scattered receivers instead the cabled receivers. We can deploy these available receivers irregularly, and obtain a corresponding sparse 3D seismic data. Compared with the desired 3D volume with regular full samples in X-, Y- and t-directions, the sparse 3D data volume from irregular point acquisition has regular full samples in the t-direction denoted by the vertical black lines, but has sparse irregular samples in X-Y directions as illustrated by the

scattered dots. In the same way as for the irregular line acquisition, we also present three reconstruction methods for irregular point acquisition illustrated in Fig. 3. One method is to use a whole 3D dataset as input of compressive sensing algorithm to reconstruct the desired full data from the sparse data volume shown in Fig 3(a). The other two methods are to group the sparse samples into vertical and horizontal subsets respectively, and then reconstruct each slice individually shown in Figs. 3(b) and 3(c).

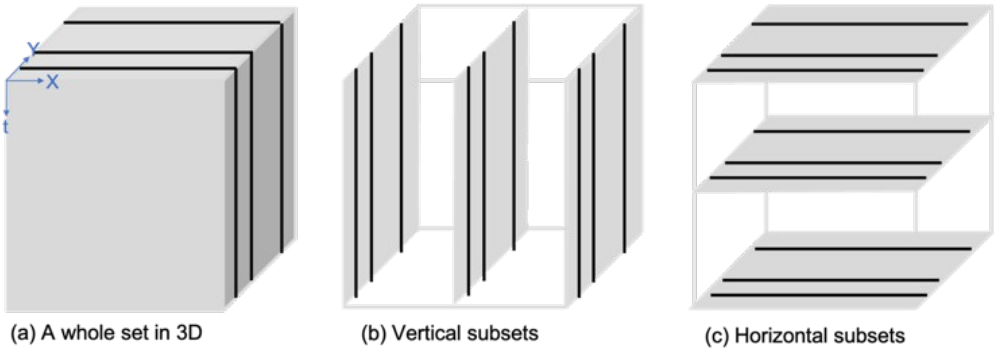

Fig. 2. Conceptual illustration of a 3D volume of seismic data from irregular line acquisition. (a) The full 3D volume of sparse samples as a whole set is equivalent to random lines in 3D, (b) When considering vertical cross-sections as subsets, the sampling pattern is equivalent to irregular lines, (c) The subsets of time slices have a sampling pattern equivalent to irregular lines too.

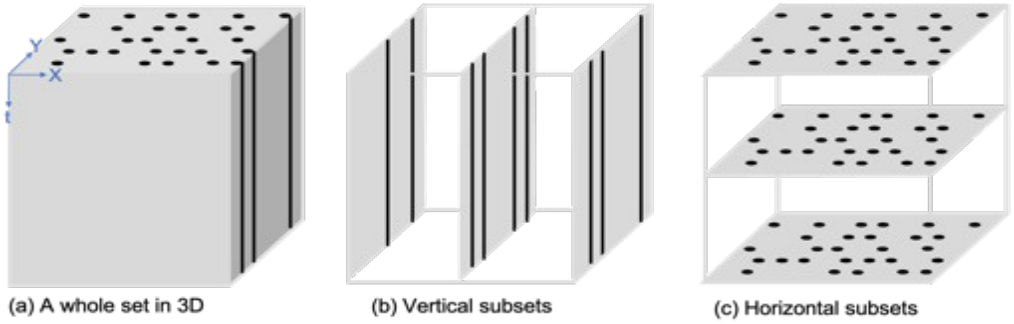

Fig. 3. Conceptual illustration of a 3D volume of seismic data from irregular point acquisition. (a) The full 3D volume of sparse samples as a whole set is equivalent to the mixture of irregular lines and irregular points in 3D. (b) When considering vertical cross-sections as subsets, the sampling pattern is equivalent to irregular lines, (c) The subsets of time slices have a sampling pattern equivalent to irregular points.

Overall, we design two types of sparse acquisition patterns: irregular line and irregular point. For each of two acquisition designs, we develop

three post-acquisition reconstruction methods from the whole 3D samples, from the vertical subsets and from the horizontal subsets. We test and compare a total of six reconstruction strategies.

SIX RECONSTRUCTION STRATEGIES USING COMPRESSIVE SENSING

Following the establishment of the two sparse acquisition designs and three different reconstruction methods, we now have six potential reconstruction strategies shown in Fig. 4. For a shot gather, we can obtain two sparse shot gathers from two irregular acquisitions, i.e., irregular lines and irregular points. For each acquisition, we apply three different reconstruction strategies: vertical subsets, a whole set, horizontal subsets. After implementing the same compressive sensing reconstruction algorithm with different input dataset, we will obtain six different reconstructions of the shot gather. We also conduct the reconstruction for all shot gathers and perform RTM to obtain six different imaging results. We then check our predictions of qualities for all reconstructed shot gathers and RTM images obtained from workflow in Fig. 4.

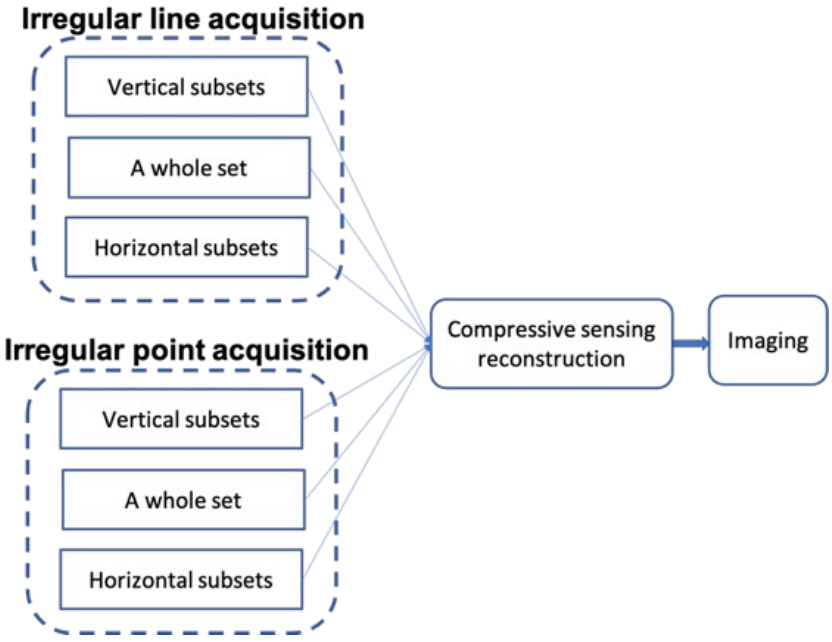

Fig. 4. Workflow from sparse acquisition to imaging. We apply two types of irregular acquisitions: line-based and point-based. For each acquisition, there are three strategies to reorganize the dataset. Therefore, we obtain six different data input. We then implement compressive sensing reconstruction algorithm and RTM imaging, and will have six reconstruction results and six imaging results for comparison.

Review of compressive sensing algorithm

Given that our investigation and demonstration depend on the use of compressive sensing reconstruction of shot gathers, we first briefly introduce compressive sensing algorithm here. Compressive sensing is a method to reconstruct a signal from a sparse set of samples (Donoho, 2001; Candès and Tao, 2006; Candès et al., 2006). Let be the sparse samples, ☞ is the sampling pattern, is the reconstruction result over a fine grid we are looking for. Compressive sensing formulates an optimization problem (Candès and Boyd, 2008),

(1)

where ✡ is a transform operator, and we use total variation (Rudin, 1992) in this paper. To minimize L1-norm objective function, we apply primal logarithmic barrier method (Nocedal and Wright, 1999; Candès and Romberg, 2005) to solve eq. (1). The primal logarithmic barrier method has been used previously for geophysical inversions with inequality constraints (e.g., Li and Oldenburg, 2003). The compressive sensing theory states that we can reconstruct from the sparse samples with a high probability as long as ☞✡ satisfies the restricted isometry property (RIP) (Candès et al., 2006). ┌ is an error parameter associated with noise level in the samples .

Sampling pattern, transform operator and optimization algorithm are three essential parts of compressive sensing. Presently, most applications in seismology focus on either the different optimization algorithms (Li et al., 2017), or different transforms (Herrmann et al., 2009), however, not much work is done to the sampling pattern, which is significant in acquisition design. Our work in this paper focuses on sampling pattern in compressive sensing.

To reconstruct the 3D seismic data from two sparse acquisitions using compressive sensing algorithm, we fix the transform operator ✡ in equation 1 and use the same optimization algorithm, different sampling pattern ☞ will lead to different reconstruction accuracy for the signal . We will check the reconstruction accuracies using SEAM data later.

COMPARISON OF SIX STRATEGIES FROM SPARSE ACQUISITIONS

For these six reconstruction strategies, there are some similarities among them. We can conceptually catalog these into different sampling patterns in reconstruction stage as shown in Fig. 5 (Zhang and Lumley, 2019): (a) irregular lines, (b) mixture of irregular lines and irregular points, (c) irregular points. Six acquisition-reconstruction strategies have been cataloged into three sampling patterns when using compressive sensing reconstruction algorithm. We define a spectral resolution function in the

following to check the reconstruction performance of these three sampling patterns.

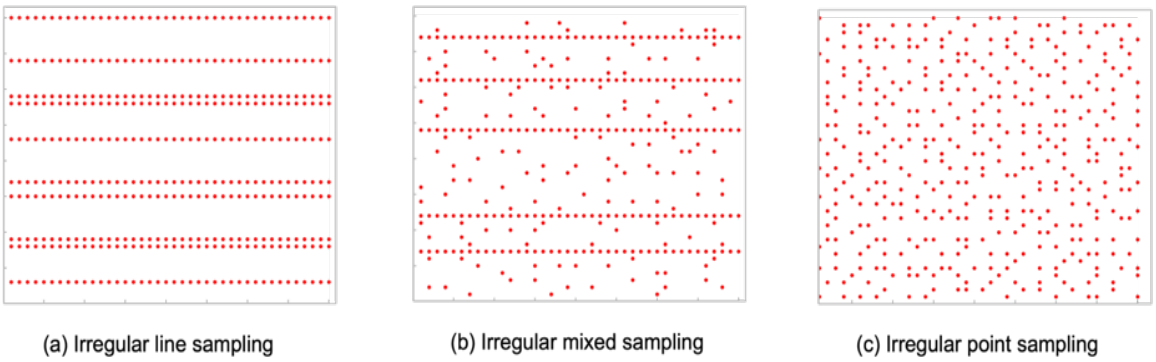

Fig. 5. Three different sampling patterns (Zhang and Lumley, 2019). (a) The sampling pattern of irregular lines, (b) the sampling pattern of mixture of irregular lines and irregular points, (c) the sampling pattern of irregular points.

Spectral resolution function (SRF)

For these three sampling patterns, it is hard to directly compare them. We define a Spectral resolution function (SRF) to check the performance of different sampling patterns. We denote sampling pattern to be Φ, and define Spectral resolution function (SRF) as,

, (2)

where is the Fourier transform, –1 denotes the inverse, and are indices denoting the positions within the SRF in the 2D Fourier domain after sparse sampling pattern. is the test signal, which has single spike at the location of in the 2D Fourier domain, and can be inverse transformed to a sinusoid signal in the space domain.

We illustrate SRF using Nyquist full sampling and sparse regular sampling pattern in Figs. 6 and 7 separately. Fig. 6 illustrates the SRF when the sampling pattern ☞ satisfies Nyquist theory. The original signal is a single sinusoid in the space domain [Fig. 6(b)], and its corresponding representation in the wavenumber domain is a single spike [Fig. 6(a)]. After applying full Nyquist sampling [Fig. 6(c)], we have the samples in Fig. 6(d) and obtain the SRF in Fig. 6(e). The SRF of a full sampling pattern is a single spike as in Fig. 6(e), i.e., there are no artifacts and when and .

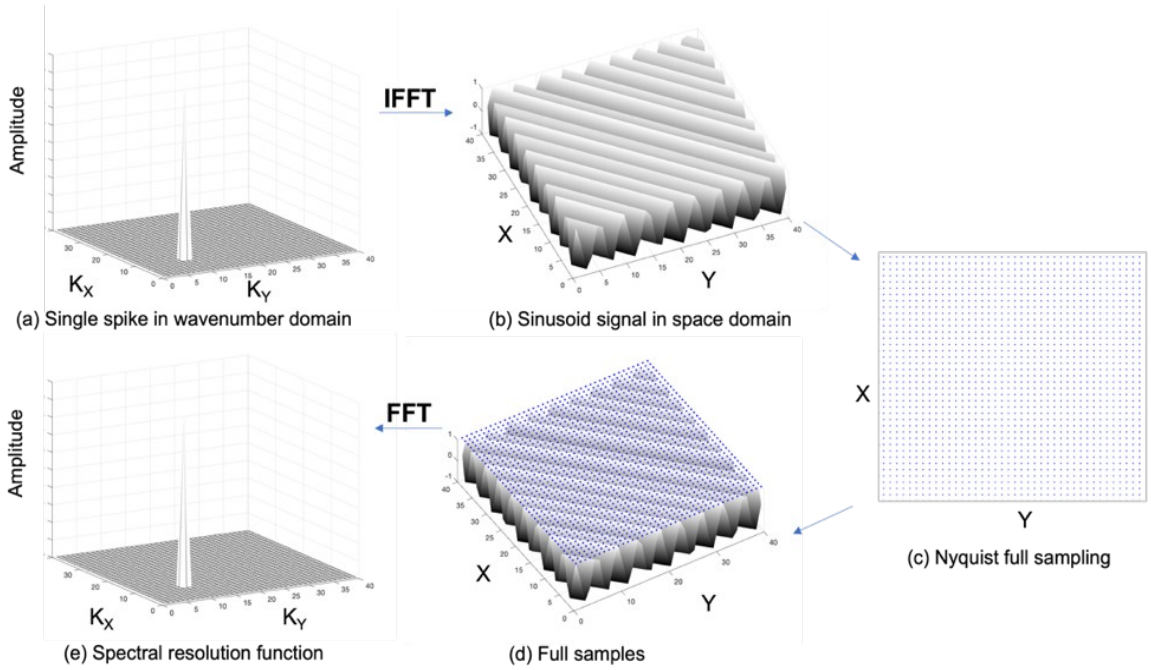

Fig. 6. (a) A single spike over a zero background, it is the 2D Fourier transform of the sinusoid signal in (b). (c) The sampling pattern: Nyquist full samples (d) sparse samples overlaid on the original sinusoid signal, (e) the SRF of the full sampling pattern.

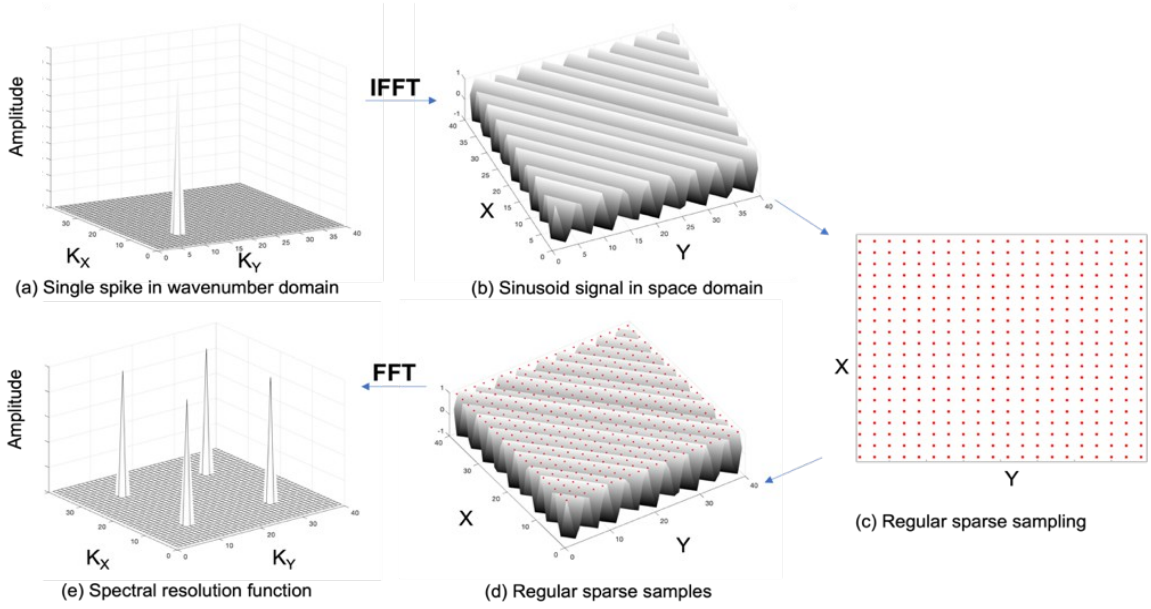

Fig. 7. (a) and (b) are the same single spike and the 2D sinusoid signal as in Fig. 6(a) and 6(b), (c) the sampling pattern: regular sparse samples, the subsampling ratio is 25%. (d) sparse samples overlaid on the original sinusoid signal, (e) the SRF of the regular sparse sampling pattern.

We want to acquire fewer samples than those required for full Nyquist sampling, so we next examine the SRF of different sparse regular sampling patterns. Following the same approach as in Fig. 6, we test the sparse regular sampling pattern in Fig. 7. After applying sparse regular sampling [Fig. 7(c)], we have the samples in Fig. 7(d). We fill the missing points with zeros and then apply an FFT to obtain the SRF in Fig. 7(e). The SRF of a regular sparse sampling pattern shows significant aliasing as shown in Fig. 7(e). Compared with the full samples satisfying Nyquist theory, this case of sparse regular sampling below Nyquist, generates artifacts and when and .

The above two examples show two extreme situations: one has zeros artifacts, and the other has artifacts that are significant enough to completely mask the true coefficient in the wavenumber domain. The SRF in this context quantifies the strengths and distributions of artifacts in the wavenumber domain, and we can use SRF to measure the leak of a unit impulse in 2D Fourier domain after a sparse sampling pattern is applied. Such a definition of is useful for understanding the resolution in the wavenumber domain and measuring the performance of sparse sampling pattern ☞ in space domain.

To be used as an indicator to evaluate the performance of different sampling pattern ☞, the definition of SRF in this paper is slightly different from the definition of similar quantities by other authors (Herrmann, 2009; Zhang and Lumley, 2019). The incoherence parameter defined by Herrmann (2009) involves the transform matrix to estimate the performance of compressive sensing, and the randomness function defined by Zhang and Lumley (2019) focuses on the reconstruction algorithm. However, since we focus on acquisition design in this paper, we define SRF to assess the performance of sampling patterns. It is reasonable that the evaluation of sampling patterns does not depend on the reconstruction algorithm. With such a definition, we can use SRF to evaluate and compare the sampling patterns themselves.

We note that SRF is similar to the wavenumber response used by Naghizadeh and Sacchi (2010). However, we use SRF only to analyze the characteristics of sampling pattern in this work and employ a different transform for reconstruction (i.e., total variation). Fourier transform is a good spectral analysis tool, but not an ideal transform to be used in reconstruction stage. Since compressive sensing reconstruction requires sparse coefficients in the transform. For general signals, Fourier coefficients are not sparse, which means that we may produce non-ideal reconstruction results. Therefore, in our work the Fourier transform is used as an analysis tool, but not used in the stage of reconstruction.

Analysis using SRF

We calculate the SRFs of the three different sampling patterns: irregular lines, irregular points, and a mixture of irregular lines and points shown respectively in Figs. 8, 9 and 10. Compared with the regular sparse sampling in Fig. 7, the sampling pattern of irregular lines in Fig. 8 shows different amplitude and distribution of artifacts in the wavenumber domain. The true coefficient, which is the largest spike in the SRF, stands out and can be identified against the small background artifacts. We notice that the artifacts of SRF in Fig 8(e) show up only in the k_X-direction, and this phenomenon is consistent with the sparse samples in the X-direction from the irregular line pattern. Compared with the sparse regular pattern, the irregular line pattern improves the resolution in the wavenumber domain since the true coefficient stands out. However, there exists some large artifacts degrading the resolution, and these artifacts may be mistaken as true coefficients. If we adjust the sampling pattern to be distributed more broadly in two directions, such as the pattern of the mixture of irregular lines and irregular points in Fig. 9(c), the energy of artifacts in the SRF can be spread out more as shown in Fig. 9(e), and we can detect the true spike more easily. Using the same number of samples as the above two patterns, the sampling pattern of irregular points makes the energy of artifacts in SRF distribute evenly, and we can identify the true coefficient much more easily.

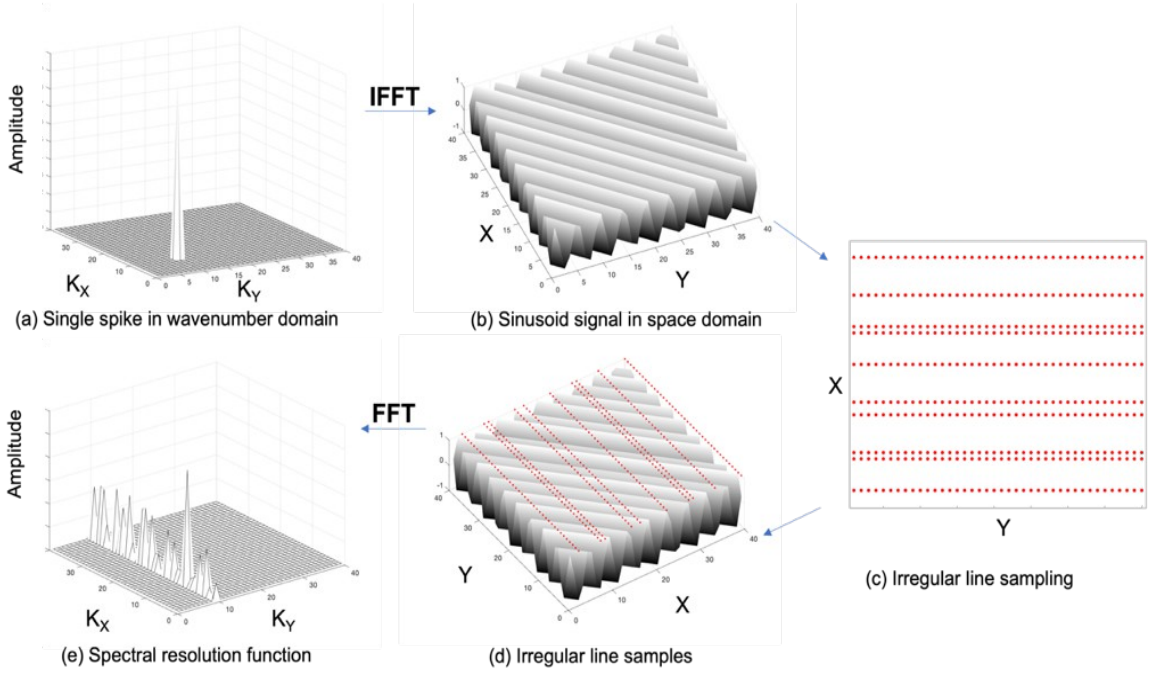

Fig. 8. (a) and (b) are the same single spike and the 2D sinusoid signal as in Figs. 6(a) and 6(b), (c) the sampling pattern: irregular lines, the subsample ratio is 25%. (d) Sparse samples overlaid on the original sinusoid signal, (e) the SRF of the sampling pattern of irregular lines.

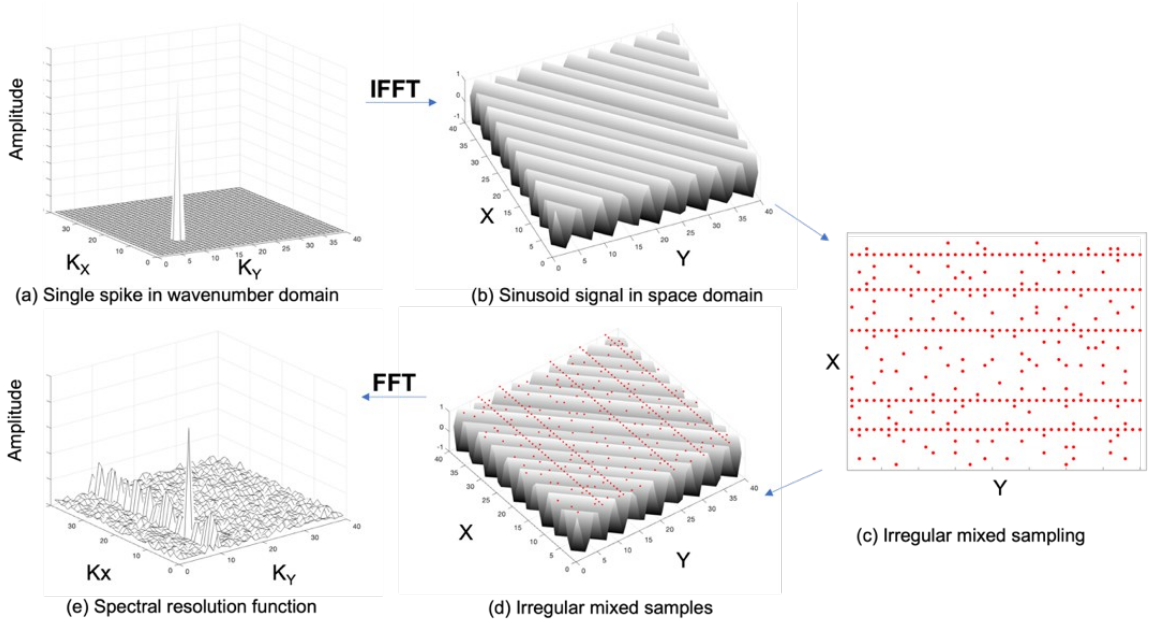

Fig. 9. (a) and (b) are the same single spike and the 2D sinusoid signal as in Figure 6(a) and (b), (c) the sampling pattern: mixture of irregular lines and irregular points, the subsample ratio is 25%. (d) sparse samples overlaid on the original sinusoid signal, (e) the SRF of the sampling pattern of mixture of irregular lines and irregular points.

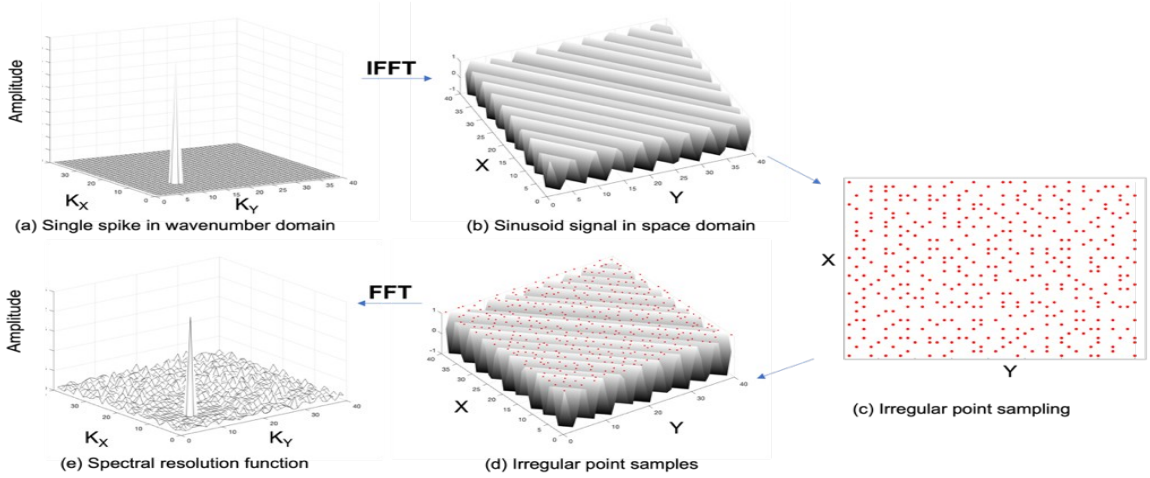

Fig. 10. (a) and (b) are the same single spike and the 2D sinusoid signal as in Figure 6(a) and (b), (c) the sampling pattern: irregular points, the subsample ratio is 25%. (d) sparse samples overlaid on the original sinusoid signal, (e) the SRF of the sampling pattern of irregular points.

Fig. 10 shows that the sampling pattern of irregular points allow the controllable artifacts to distribute evenly in SRF, making the amplitudes of artifacts much smaller than that of the true coefficients. The SRF in Fig. 10(e) most resembles the SRF of Nyquist full sampling in Fig. 6(e), and has the highest resolution in the wavenumber domain among these three

sampling patterns. Among these three sampling patterns, it is worth to mention that SRF from the mixture of irregular lines and points has weaker artifacts than that of irregular lines, but stronger than that of the irregular points, so the irregular line pattern has the least performance, then the mixture pattern is in the middle, and the irregular point pattern performs best

SRF can rank the performance of different sampling patterns and indicate the expected reconstruction accuracy related to these sampling patterns. Based on SRF, we will analyze the six reconstruction strategies from sparse acquisition.

PREDICTION OF RECONSTRUCTION ACCURACIES FROM SPARSE ACQUISITIONS

Based on the sampling pattern analysis using SRF, we rank the total six reconstruction strategies from two irregular acquisitions. We can predict the accuracies of reconstructed data and rank them as in Table 1.

For the irregular line acquisition in the left column of Table 1, the reconstruction from vertical and horizontal subsets should have the least accuracy (one star) since their sampling pattern is irregular lines. It is also expected that the reconstruction from a whole set has better accuracy (two stars), since we involve more data to generate the reconstruction result. For the irregular point acquisition in the right column of Table 1, three reconstruction strategies show interesting differences in the reconstruction accuracy. When we divide the sparse samples into vertical subsets, the sampling pattern for each cross-section is analogous to irregular lines (Fig. 8), which has the least spectral resolution in the wavenumber domain. Therefore, the reconstruction using these cross-sections should be the least accurate (one star). If we divide samples into horizontal subsets, the sampling pattern for each subset is equivalent to that of irregular points (Fig. 10), which has the best spectral resolution function. Therefore, the reconstruction accuracy using time-slices should be the best (four stars).

The sampling pattern with a mixture of irregular lines and points in the middle of right column has an interesting but counter-intuitive property. On one hand, when we use the whole 3D dataset for reconstruction, we expect to achieve the best reconstruction accuracy since we input as much data as possible. One the other hand, the sampling pattern analysis above shows that this mixture sampling pattern has an intermediate performance among the three sampling patterns, and can only reach the middle level of reconstruction accuracy. We predict that sampling patterns contribute more to reconstruction than the amount of data. We will test this prediction later on 3D seismic dataset.

Table 1. Two sparse acquisitions with irregular line and irregular point are in the two columns. The three different reconstruction strategies are in the rows. These six reconstructions are cataloged into different sampling patterns. Based on the SRF analyses, we predict the quality level of the reconstructed data and mark the reconstruction accuracy with stars.

Geometry / Reconstruction	Irregular line design	Irregular point design
Vertical subsets	★ (line pattern)	★(line pattern)
A whole set in 3D	★★(line pattern)	★★★(mixed pattern)
Horizontal subsets	★(line pattern)	★★★★(point pattern)

In addition, we have several predictions for each row in Table 1. For the reconstruction strategy with vertical subsets in the first row, the two acquisitions should have the similar reconstruction accuracy (one star) since both of them have the sampling pattern of irregular lines. When we use the reconstruction strategy with a whole set in 3D, we input the same amount of data, but employ different sampling patterns. Compared with the sampling pattern of irregular lines in the irregular line acquisition, the sampling pattern of reconstruction strategy in irregular point acquisition is analogous to the mixture of irregular lines plus irregular points. Thus, the mixed sampling pattern in sparse point acquisition should have better reconstruction accuracy. The results are more interesting when we use the reconstruction strategy with horizontal subsets. The reconstruction result with such subsets in the irregular point acquisition should be the best among all six reconstruction results.

In summary, we have analyzed two types of sparse acquisition designs, which are suitable for different physical configurations of receivers. For the cabled receivers which can only been deployed in the pattern of irregular lines such as ocean bottom cables (OBC), the reconstruction strategy using a whole set in 3D would produce better result. For the scattered receivers which can be arranged in the pattern of irregular points such as ocean bottom nodes (OBN), the reconstruction method using horizontal subsets should produce the best reconstruction accuracy.

Moreover, there are two advantages to the reconstruction strategy by dividing the sparse samples into horizontal subsets in the irregular point acquisition. The first is that the subsets of time slices generate the sampling pattern with a high resolution in the wavenumber domain, and can facilitate the most accurate reconstruction of the 3D seismic volume. In contrast to

reconstruction in 3D using all sparse data samples, the reconstruction by 2D time slices solves a 3D problem with multiple 2D problems. As a results, this approach is also computationally much more efficient.

RECONSTRUCTION TESTS AND IMAGE DEMONSTRATIONS

Following the sampling pattern analysis and reconstruction accuracy predictions in Table 1, we now demonstrate and verify the predictions using a synthetic SEAM seismic data set (Oppert et al., 2017). We first demonstrate the predictions in Table 1 using one shot gather by implementing different reconstruction strategies from two sparse acquisitions. We will then apply reconstructions to all simulated sparse shot gathers, implement RTM, and compare the accuracies of these images.

Shot gather reconstructions

We first test different reconstruction strategies using equation 1 on one shot gather and compare the accuracies of these reconstructions. ε is set to be zero since SEAM data has no noise. In the case of noisy data, L-curve (Hansen, 1992) is a good approach to estimate the ε value. In this paper, we use total variation as the transform operator and logarithmic barrier method as optimization algorithm as stated earlier.

Fig. 11(a) shows a 3D shot gather from SEAM data, and Figs. 11(b) and 11(c) are one time-slice and one cross-section. We will reconstruct this 3D shot gather by using only 25% of the full receivers to simulate low-cost acquisitions. We deploy these receivers to form irregular line or irregular point acquisition as illustrated in Fig. 1. We then obtain three reconstructed seismic shot gathers from each of the two sparse acquisitions. The total of six reconstructed shot gathers are displayed at the same time-slice in Fig. 12 and in a cross-section in Fig. 14.

In Fig. 12, the reconstructions in the left column come from the irregular line acquisition, and the reconstructions in the right column come from the irregular point acquisition. Meanwhile, the reconstructions using the vertical subsets are shown in the first row, the whole set in the second row, and horizontal subsets in the third row. We have already done theoretical analyses about the reconstruction accuracy shown in Table 1, and have ranked the expected reconstruction accuracies. Here we verify the prediction with the reconstruction results from one shot gather.

We can observe that the reconstructed seismic events are blurry in Figs. 12(a), 12(b) and 12(e), since the sampling pattern is irregular lines in these reconstructions. These reconstructions are the least accurate, which is consistent

with our predictions in Table 1. Although the corresponding sampling pattern in Fig. 12(c) is irregular lines, we obtain a better reconstruction result because we input more data into the compressive sensing algorithm when using the whole set. In contrast to Fig. 12(c), Fig. 12(d) treats all samples as one set in 3D, the corresponding sampling pattern is analogous to a mixture of irregular lines and irregular points. As predicted, the reconstruction in Fig. 12(d) has a better accuracy than that in Fig. 12(c). Fig. 12(f) is the reconstruction from dividing samples into horizontal subsets when using irregular point acquisition. The sampling pattern in each time slice is equivalent to irregular points, so we can obtain the most accurate reconstruction. We can observe that the reflection events are reconstructed well and the reconstruction accuracy in Fig. 12(f) is the best.

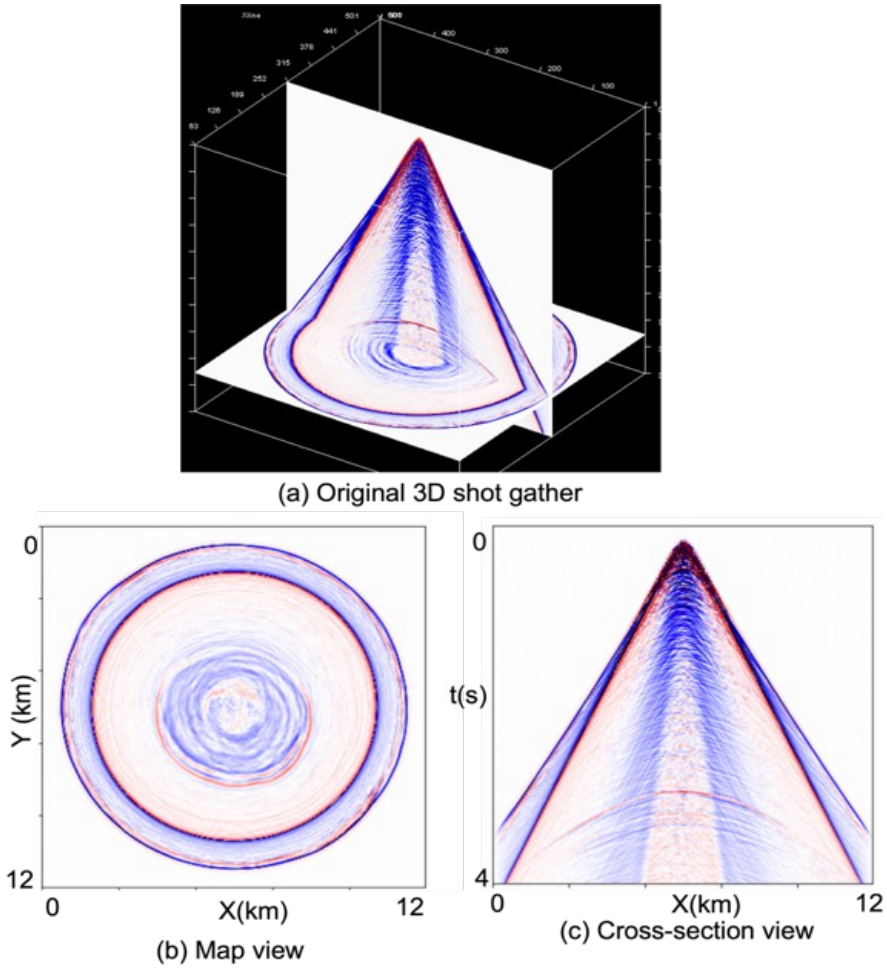

Fig. 11. (a) SEAM 3D shot gather, (b) map-view of one time slice, (c) cross-section view.

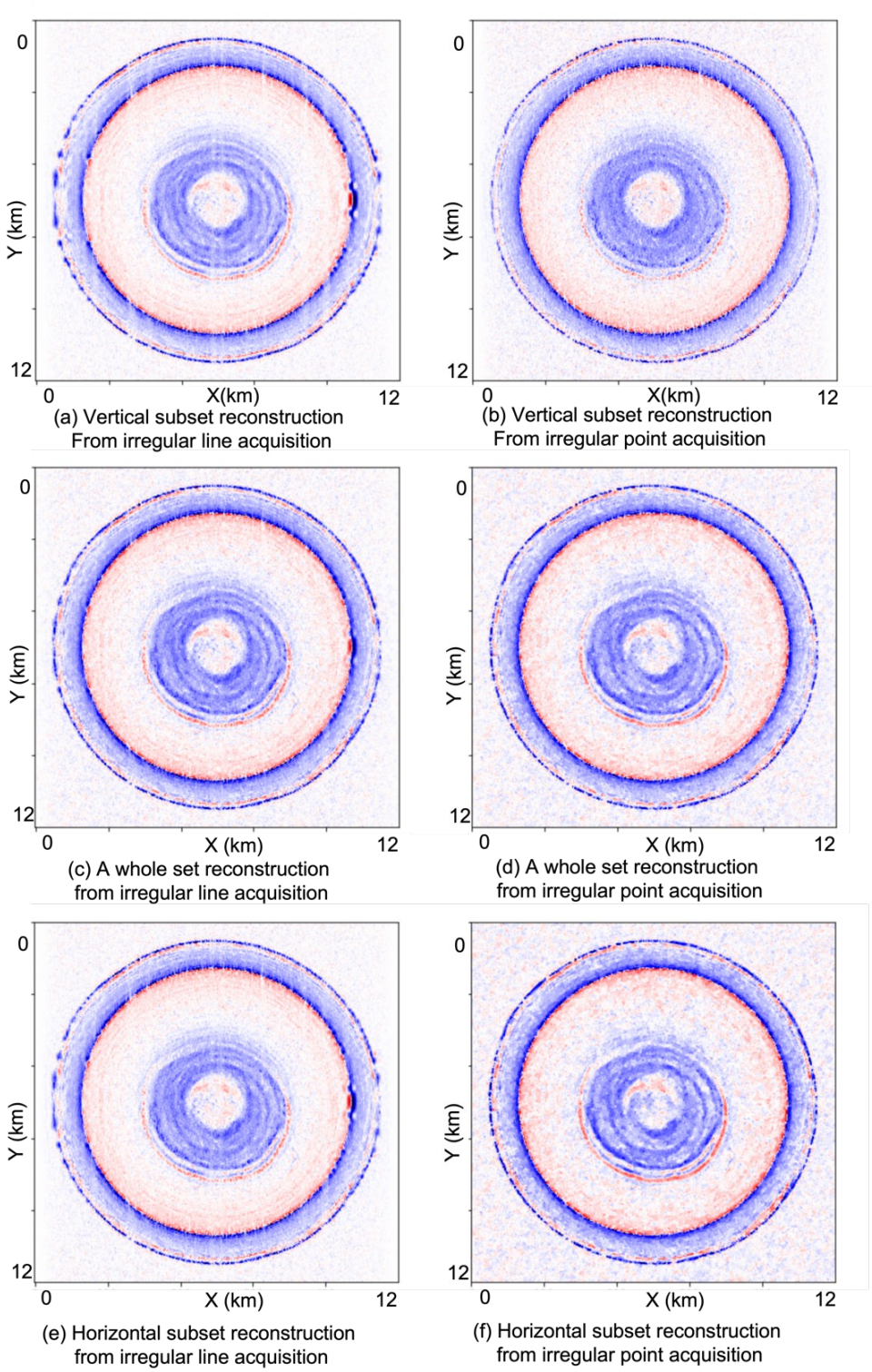

Fig. 12. Map-view of reconstruction examples of 3D single shot gather from 25% receivers. On the left column is irregular line acquisition, on the right column is irregular point acquisition. The reconstructions use the vertical subsets in the first row, the whole set in the second row and the horizontal subsets in the third row.

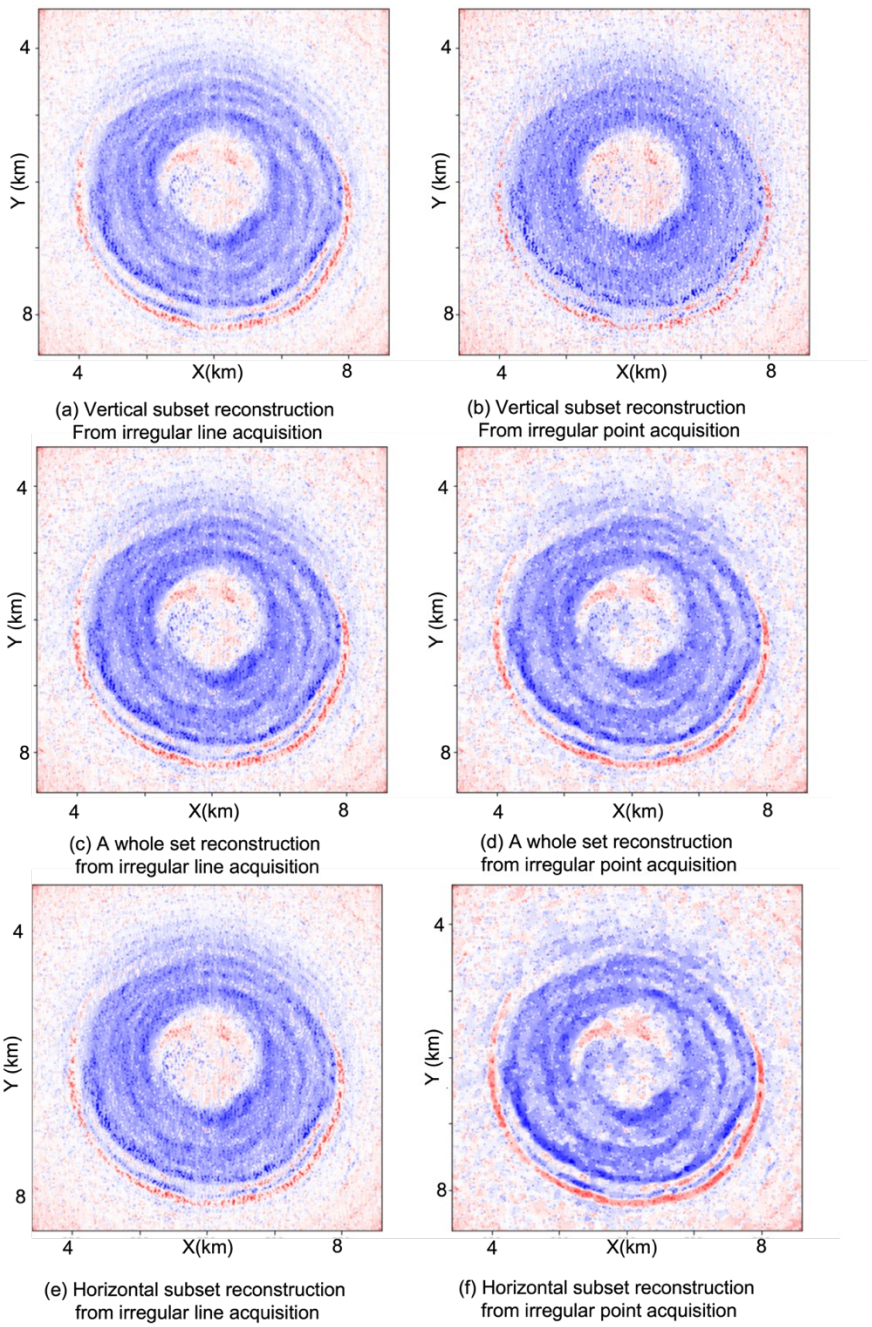

Fig. 13. Detailed display of reconstruction at reservoir locations from Figure 12. On the left column is irregular line acquisition, on the right column is irregular point acquisition. The reconstructions use the vertical subsets in the first row, the whole set in the second row and the horizontal subsets in the third row.

Fig. 13 is a zoomed-in map-view display of reflection events near the reservoir. We can observe that three reconstructions in the left column from irregular line design have slight stripe-like artifacts, especially the reconstructions in Figs. 13(a) and 13(e). The reason is that the irregular line

sampling acquires redundant information along its lines, but misses information across the lines. Therefore, irregular lines generate poorer reconstructions. In contrast, the irregular point sampling uses the same number of samples, but acquire more information than does the irregular line sampling with the same number of samples.

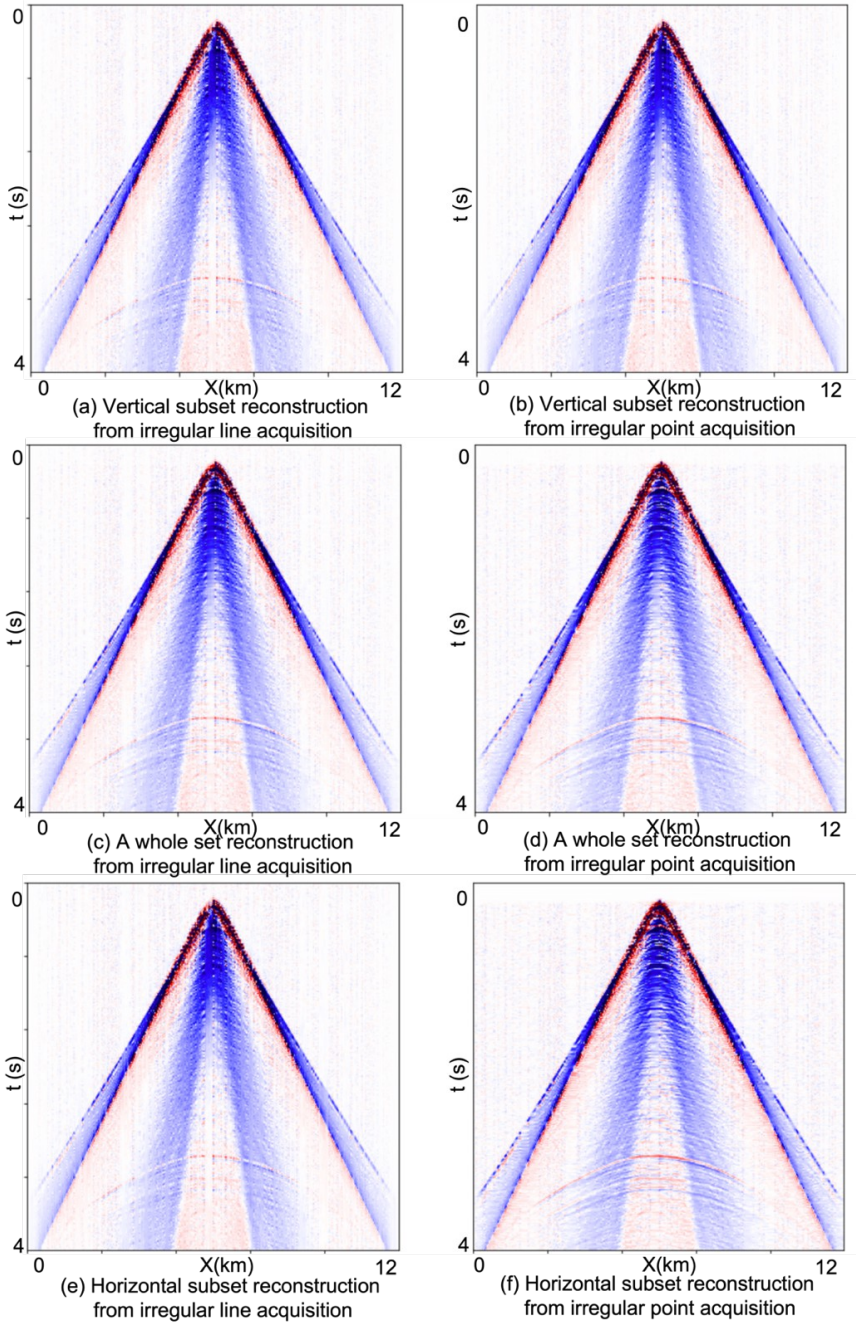

Fig. 14. Cross-section view of reconstruction examples of 3D single shot gather from 25% receivers. On the left column is irregular line acquisition, on the right column is irregular point acquisition. The reconstructions use the vertical subsets in the first row, the whole set in the second row and the horizontal subsets in the third row.

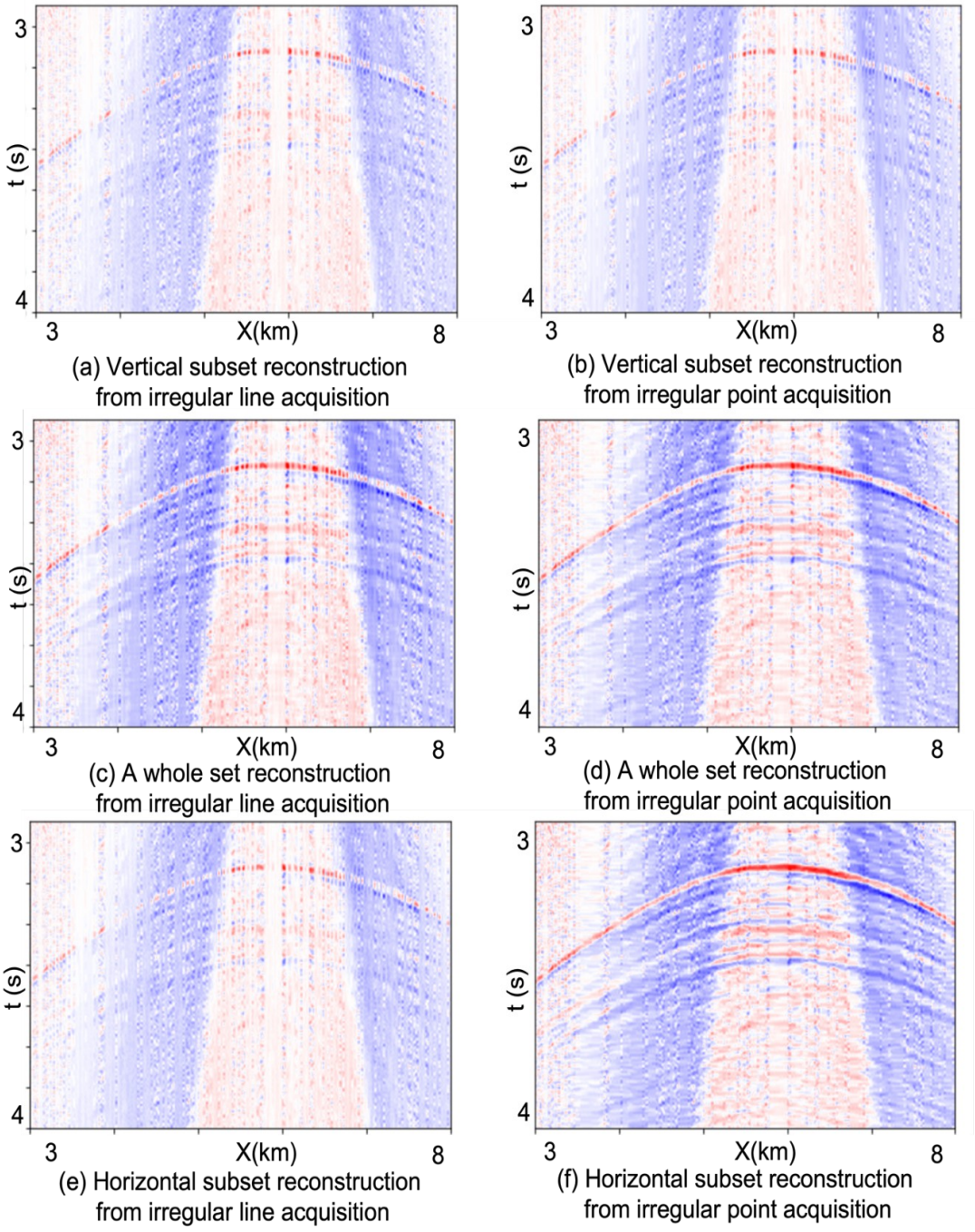

Fig. 15. Detailed display of reconstruction at reservoir locations from Fig. 14. On the left column is irregular line acquisition, on the right column is irregular point acquisition. The reconstructions use the vertical subsets in the first row, the whole set in the second row and the horizontal subsets in the third row.

The reconstructed 3D shot gathers shown by the cross-section view in Fig. 14 are also consistent with Table 1. We can observe that the reflection events containing the reservoir information become clearer in the reconstructions as indicated by Table 1. The sampling pattern in Figs. 14(a), 14(b), and 14(e) is equivalent to irregular lines and has the least resolution in the wavenumber domain. Therefore, as predicted, the reconstructed hyperbolic reflection events are blurry. The sampling pattern in Fig. 14(d) is analogous to a mixture of irregular lines and irregular points. As predicted, the reconstruction in Fig. 14(d) has an intermediate accuracy. The sampling pattern in Fig. 14(f) is irregular points, and the hyperbolic reflection events in this reconstruction shows up most clearly among the six reconstructions. The sampling pattern has a significant influence on the reconstruction accuracy. There is a trade-off between the amount of data and sampling pattern. If we input more data but have to use a sampling pattern with poor spectral resolution, we will degrade the reconstruction results.

Fig. 15 is a zoomed-in display of reflection events near the reservoir between 3 s and 4 s. We can observe that, with different sampling patterns, the reflection events appear differently in the reconstructions. Meanwhile, stripe-like artifacts showing up in all reconstructions is caused by the big gap between lines. This phenomenon is also illustrated in the papers by Pawelec et al. (2021) and Zhang (2021). To further improve the reconstruction results, more investigations on SRF and different combinations of compressive sensing components could be needed. However, among all the results in Figs. 15, the reconstruction using the horizontal subsets from irregular point acquisition has the least signal leakage and the smallest residual, and shows more clearly the hyperbolic shape of the reflection events. There is also an added benefit of reduced computational cost when reconstructing using these subsets.

Migration imaging

The preceding subsection has demonstrated that we can reconstruct shot gathers from sparsely located receivers. The goal of obtaining these shot gathers is to image the sub- surface. We therefore examine the feasibility of performing migration imaging using such reconstructed gathers in this section.

We repeat the reconstructions for 15 SEAM 3D shot gathers using 25% receivers with all shots along a line, and obtain six sets of reconstructed data. Next, we apply reverse time migration (RTM) to the data with full receivers and to these six different sets of reconstructed shot gathers. For brevity and for ease of presentation, we extract 2D shot gathers from these 3D gathers and apply a 2D RTM imaging. We obtain two sets of 2D RTM imaging results. The first section is located at a part of a reservoir that is continuous

(Fig. 16); and the second cuts through the reservoir with a normal fault (Fig. 17).

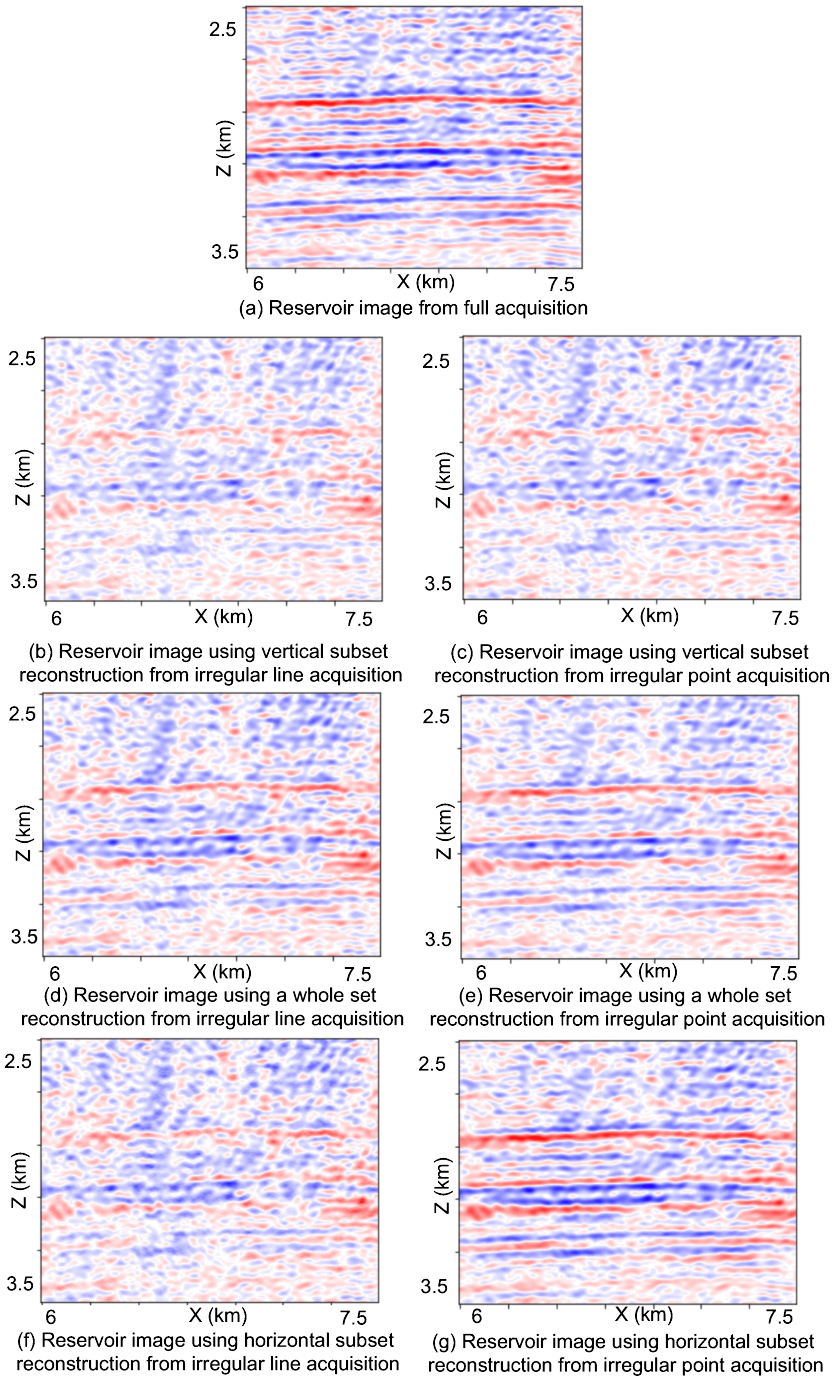

Fig. 16. Images from SEAM synthetic data by using reverse time migration to illustrate the reservoir location. (a) the original reservoir image, (b), (d) and (f) are reservoir images using different reconstructed methods from irregular line acquisition. (c), (e) and (g) are reservoir images using different reconstructed methods from irregular point acquisition. The reservoir in

Figure (g) using horizontal subsets from irregular point acquisition is the most accurate.

Fig. 16 illustrates the comparison of images with the continuous part of the reservoir. Fig. 16(a) is the reservoir image using the full acquisition. Figs. 16(b), 16(d) and 16(f) are the reservoir images using three different reconstruction strategies from the irregular line acquisition. Figs. 16(c), 16(e), and 16(g) are the reservoir images using three different reconstruction strategies from the irregular point acquisition. We can observe that the reservoir is obscured and difficult to detect in Figs. 16(b), 16(c) and 16(f), because the quality of the data reconstruction is low as predicted in Table 1. Based on the previous sampling pattern analyses, the vertical subset is equivalent to irregular lines, the reconstruction is the least accurate and will lead to low resolution imaging. Although the sampling pattern is still irregular lines, the reservoir image in Fig. 16(d) is better because more data is input into the compressive sensing algorithm. Compared with Fig. 16(d), Fig. 16(e) uses the whole set too, but the sampling pattern is mixture of irregular line and irregular points, therefore, the RTM image shows the reservoirs more clearly. The reservoir image in Fig. 16(g) is the most clear as we have predicted in Table 1. The reason is that the sampling pattern is irregular points when using the horizontal subsets in the irregular point acquisition.

We next examine comparison of images of the faulted part of the reservoir in Fig. 17. The RTM image using full acquisition is shown in Fig. 17(a). Figs. 17(b), 17(d) and 17(f) are the images using three different reconstructed strategies from the irregular line acquisition. Figs. 17(c), 17(e) and 17(g) are the reservoir images using three different reconstruction strategies from the irregular point acquisition. It is nearly impossible to identify a fault in Figs. 17(b), 17(c) and 17(f), and we would likely interpret a seismic reservoir event without the faulting. However, we are able to detect the fault in Figs. 17(d), 17(e) and 17(g). This normal fault can be identified most easily in Fig. 17(g). These results are expected from Table 1.

The results in these two sets of images demonstrate the consistence with our prediction in Table 1. For the irregular line acquisition such as when using OBC, reconstruction as a whole set is a good choice. For the irregular point acquisition such as when using OBN, the reconstruction using horizontal subsets is the best scenario. Therefore, a suitable combination of acquisition design and corresponding reconstruction strategy can produce a better imaging result. Moreover, an irregular point acquisition is preferable to an irregular line acquisition, since using horizontal subsets for the reconstruction in the irregular point acquisition can improve both accuracy and computational efficiency.

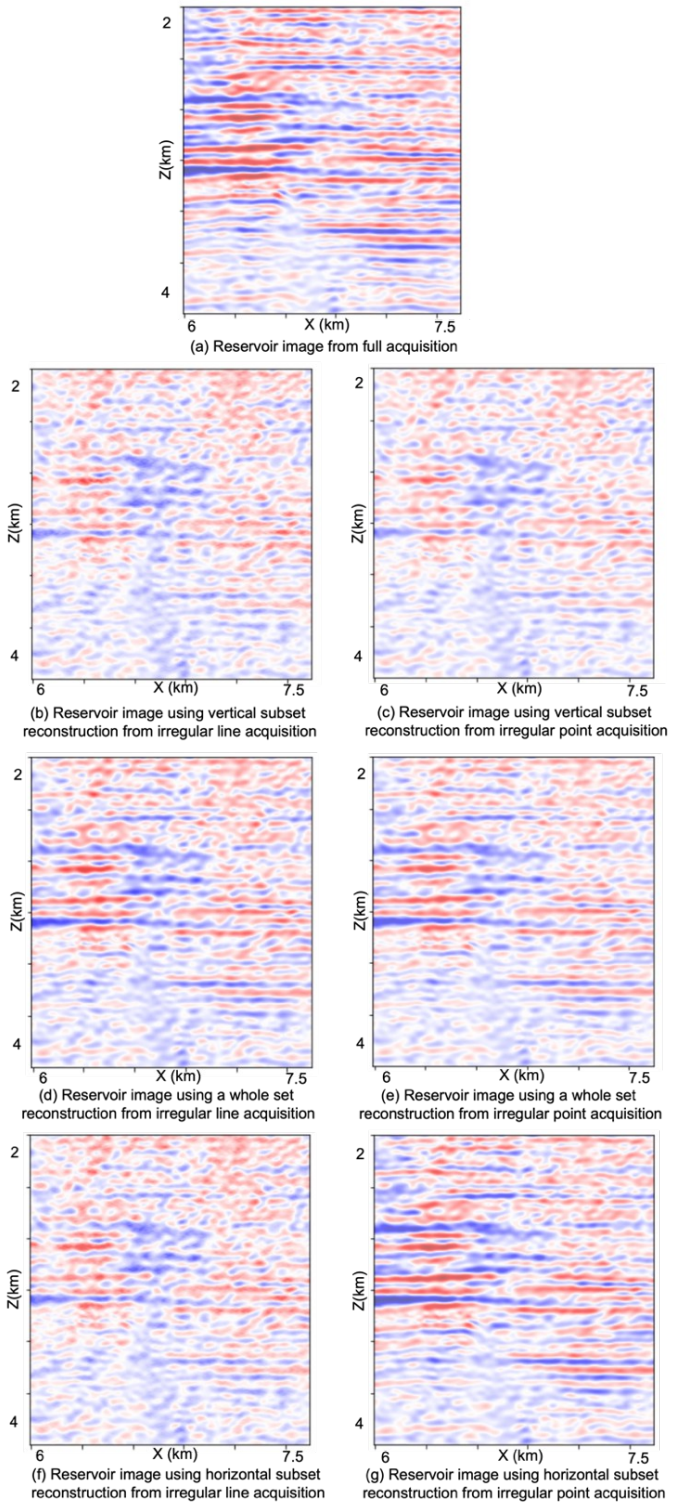

Fig. 17. Images from SEAM synthetic data by using reverse time migration to illustrate the fault location. (a) the original reservoir image, (b), (d) and (f) are reservoir images using different

reconstructed methods from irregular line acquisition. (c), (e) and (g) are reservoir images using different reconstructed methods from irregular point acquisition. The fault in Fig. (g) using horizontal subsets from irregular point acquisition is the most detectable.

CONCLUSION

We have investigated two types of sparse seismic acquisition designs, namely irregular lines and irregular points that simulate respectively OBC and OBN. For each acquisition design, we have also developed different compressive sensing reconstruction strategies using different subsets of the samples. Our sampling pattern analyses based on Spectral Resolution Function (SRF) can help improve the acquisition design and predict the reconstruction accuracy. Our studies predict that in irregular line acquisition, it is better to use the whole dataset to reconstruct shot gathers; while in irregular point acquisition, it is best to use horizontal subsets in the reconstruction. The simulations using SEAM seismic dataset to reconstruct shot gathers and implement RTM demonstrate the consistency with prediction from our studies. We demonstrate that the compressive sensing acquisition design and compressive sensing post-acquisition reconstruction can use different transforms. A good combination of sampling pattern, transform, and optimization algorithm can reduce the required samples to 25%. Our work highlights the importance of the acquisition designs and sampling pattern analyses in the sparse acquisition, and illustrates that compressive sensing acquisition can play an important role in high resolution data acquisition with low cost.

ACKNOWLEDGMENTS

I appreciate Dr. Yaoguo Li for the helpful discussion. I thank the SEAM time-lapse Pilot data provided by the Center for Gravity, Electrical, and Magnetic Studies (CGEM) at Colorado School of Mines.

REFERENCES

Abma, R., Howe, D., Foster, M., Ahmed, I., Tanis, M., Zhang, Q., Arogunmati, A. and Alexander, G., 2015. Independent simultaneous source acquisition and processing. Geophysics, 80(6): WD37-WD44.

Baraniuk, R. and Kelly, K., 2007. Compressive sensing. Signal Process., 4: 12-21.

Brown, L., Mosher, C.C., Li, C., Olson, R., Doherty, J., Carey, T.C., Williams, L., Chang, J. and Staples, E., 2017. Application of compressive seismic imaging at lookout field, Alaska: The Leading Edge, 36: 670-676.

Candès, E. and Romberg, J., 2005. l1-magic: Recovery of sparse signals via convex programming: 1-19.

Candès, E.J., Romberg, J. and Tao, T., 2006. Robust uncertainty principles: exact signal reconstruction from highly incomplete frequency information. IEEE Transact. Informat. Theory, 52: 489-509.

Candès, E.J. and Tao, T., 2006. Near-optimal signal recovery from random projections: Universal encoding strategies?: IEEE Transact. Informat. Theory, 52: 5406-5425.

Candès, E.J. and Wakin, M.B.. 2008. An introduction to compressive sampling. IEEE Signal Process. Magaz., 25: 21-30.

Candès, M.W. and Boyd, S., 2008. Enhancing sparsity by reweighted l1 minimization. J Fourier Anal. Appl., 14: 877-905.

Donoho, D.L., 2001. Uncertainty principles and ideal atomic decomposition. IEEE Transact. Informat. Theory, 47: 2845-2862.

Donoho, D.L., 2006. Compressed sensing. IEEE Transact. Informat. Theory, 52. 1289-1306.

Donoho, D.L. and Tanner, J., 2010. Exponential bounds implying construction of compressed sensing matrices, error-correcting codes, and neighborly polytopes by random sampling. IEEE Transact. Informat. Theory, 56: 2002-2016.

Donoho, D.L. and Tsaig, Y., 2008. Fast solution of ˆ 1 -norm minimization problems when the solution may be sparse. IEEE Transact. Informat. Theory, 54: 4789-4812.

Donoho, D.L., Tsaig, Y., Drori, I. and Starck, J., 2012. Sparse solution of underdetermined systems of linear equations by stagewise orthogonal matching pursuit: IEEE Transact. Informat. Theory, 58: 1094-1121.

Hansen, P.C., 1992. Analysis of discrete ill-posed problems by means of the L-curve: SIAM Review, 34: 561-580. doi: 10.1137/1034115.

Herrmann, F.J., 2009. Compressive imaging by wavefield inversion with group sparsity. Expanded Abstr., 79th Ann. Internat. SEG Mtg., Houston: 2337-2341.

Herrmann, F.J., Erlangga, Y.A. and Lin, T.T., 2009. Compressive simultaneous full-waveform simulation. Geophysics, 74(4): A35-A40.

Janiszewski, F., Mosher, C., Li, C. and Malloy, J., 2017. Applying compressive sensing techniques in production offshore seismic surveys. Expanded Abstr., 87th Ann. Internat. SEG Mtg., New Orleans: 47-51.

Li, C., Mosher, C., Keys, R., Janiszewski, F. and Zhang, Y., 2017. Improving streamer data sampling and resolution via nonuniform optimal design and reconstruction, Expanded Abstr., 87th Ann. Internat. SEG Mtg., New Orleans: 4241-4245.

Li, Y. and Oldenburg, D.W., 2003. Fast inversion of large-scale magnetic data using wavelet transforms and a logarithmic barrier method. Geophys. J. Internat., 152: 251-265.

Lustig, M., Donoho, D. and Pauly, J.M., 2007. Sparse MRI: The application of compressed sensing for rapid MRI imaging: Magnetic Resonance in Medicine, 58, 1182-1195.

Lustig, M., Donoho, D.L., Santos, J.M. and Pauly, J., 2008. Compressed sensing MRI. IEEE Signal Process. Magaz., 25: 72-82.

Milton, A., Trickett, S. and Burroughs, L., 2011. Reducing acquisition costs with random sampling and multidimensional interpolation. Expanded Abstr., 81st Ann. Internat. SEG Mtg., San Antonio: 52-56.

Moldoveanu, N., 2010. Random sampling: A new strategy for marine acquisition. Expanded Abstr., 80th Ann. Internat. SEG Mtg., Denver: 51-55.

Moldoveanu, N., Bilsby, P., Quigley, J., Kumar, R. and Herrmann, F., 2018. Compressive sensing based design for land and obs surveys: The noise issue. Expanded Abstr., 88th Ann. Internat. SEG Mtg., Anaheim: 102–106.

Mosher, C.C., Keskula, E., Kaplan, S.T., Keys, R.G., Li, C., Ata, E.Z., Morley, L.C., Brewer, J.D., Janiszewski, F.D., Eick, P.M. and Olson, R.A., 2012. Compressive seismic imaging. Expanded Abstr., 82nd Ann. Internat. SEG Mtg., Las Vegas: 1-5.

Mosher, C.C., Li, C., Janiszewski, F.D., Williams, L.S., Carey, T.C. and Ji, Y., 2017. Operational deployment of compressive sensing systems for seismic data acquisition. The Leading Edge, 36: 661-669.

Naghizadeh, M. and Sacchi, M.D., 2010. On sampling functions and Fourier reconstruction methods. Geophysics, 75(**Issue No.????),** WB137-WB151.

Nocedal, J. and Wright, S.J., 1999. Numerical Optimization. Springer-Verlag, New York.

Oppert, S., Stefani, J., Eakin, D., Halpert, A., Herwanger, J.V., Bottrill, A., Popov, P., Tan, L., Artus, V. and Oristaglio, M., 2017. Virtual time-lapse seismic monitoring using fully coupled flow and geomechanical simulations. The Leading Edge, 36; 750-768.

Pawelec, I., Wakin, M. and Sava, P., 2021. Missing trace reconstruction for 2d land seismic data with randomized sparse sampling. Geophysics, 86(6): P25-P36.

Rudin, S. and Osher, C. and Fatami, E., 1992. Nonlinear total variation noise removal algorithm. Phys. D, 60: 259-268.

Tsaig, Y. and Donoho, D.L., 2006. Extensions of compressed sensing. Signal Process., 86: 549-571. (Sparse Approximations in Signal and Image Processing).

Wakin, M., Becker, S., Nakamura, E., Grant, M., Sovero, E., Ching, D., Yoo, J., Romberg, J., Emami-Neyestanak, A. and Candès, E., 2012. A nonuniform sampler for wideband spectrally - sparse environments. IEEE J. Emerg. Select. Topics Circuits Syst., 2: 516-529.

Wakin, M.B., Laska, J.N., Duarte, M.F., Baron, D., Sarvotham, S., Takhar, D., Kelly, K.F. and Baraniuk, R.G., 2006. An architecture for compressive imaging. Internat. Conf. Image Process.: 1273-1276.

Wason, H. and Herrmann, F.J., 2013. Time-jittered ocean bottom seismic acquisition. Expanded Abstr., 83rd Ann. Internat. SEG Mtg., Houston: 1-6.

Wright, S., 1997, Primal-Dual Interior-Point Methods. SIAM, Philaelphia.

Zhang, M., 2020. Marchenko Green's functions from compressive sensing acquisition. Expanded Abstr., 90th Ann. Internat. SEG Mtg., Huston: 2794-2798.

Zhang, M., 2021. Time-lapse seismic data reconstruction using compressive sensing: Geophysics, 86(3): P37-P48.

Zhang, M., 2022, Compressive sensing acquisition with application to Marchenko imaging. Pure Appl. Geophys., 179: 2383-2404.

Zhang, M. and Li, Y., 2021. Efficient ground EM acquisition using irregular sparse stations: A compressive sensing approach. Expanded Abstr., Internat. Mtg. Appl. Geosci. Energy: 1241-1245.

Zhang, M. and Li, Y., 2022. Irregular acquisition design to maximize information: From cross-lines to ergodic sampling. Expanded Abstr., Internat. Mtg. Appl. Geosci. Energy, Denver: 1150-1154.

Zhang, M. and Lumley, D., 2019. Reconstruction of 3D seismic data from sparse random OBN acquisition by compressive sensing. Expanded Abstr., 89th Ann. Internat. SEG Mtg., New Orleans: 127-130.

Zwartjes, P. and Gisolf, A., 2007. Fourier reconstruction with sparse inversion. Geophys. Prosp., 55: 199-221.